Gravity Driven Instability in Elastic Solid Layers

Serge Mora*
Laboratoire de Mécanique et de Génie Civil, UMR 5508, Université Montpellier 2 and CNRS, Place Eugène Bataillon, F-34095 Montpellier Cedex, France

Ty Phou and Jean-Marc Fromental
Laboratoire Charles Coulomb, UMR 5521, Université Montpellier 2 and CNRS, Place Eugène Bataillon, F-34095 Montpellier Cedex, France

Yves Pomeau
Department of Mathematics, University of Arizona, Tucson, Arizona 85721, USA
(Received 13 May 2014; revised manuscript received 6 September 2014; published 21 October 2014)

We demonstrate the instability of the free surface of a soft elastic solid facing downwards. Experiments are carried out using a gel of constant density ρ, shear modulus μ, put in a rigid cylindrical dish of depth h. When turned upside down, the free surface of the gel undergoes a normal outgoing acceleration g. It remains perfectly flat for $\rho gh/\mu < \alpha^*$ with $\alpha^* \simeq 6$, whereas a steady pattern spontaneously appears in the opposite case. This phenomenon results from the interplay between the gravitational energy and the elastic energy of deformation, which reduces the Rayleigh waves celerity and vanishes it at the threshold.

DOI: 10.1103/PhysRevLett.113.178301 PACS numbers: 83.80.Kn, 46.25.-y, 46.32.+x, 47.20.Ma

Many materials such as biological tissues can withstand huge elastic deformations of more than several hundred percent. The amplitude of the stress is then of the order of the elastic modulus, a situation commonly encountered with soft materials. Specific and fascinating patterns, reminiscent of those that can be seen in hydrodynamics, can then occur spontaneously [1–10]. Since both soft elastic solids and liquids are capable of undergoing large deformations, and are often subjected to forces with a common origin, e.g., capillary forces [6,11], it is likely that some mechanical instabilities can be shared, to a certain extent, by these two kinds of continuous media [3]. Out of the many instabilities experienced by liquids, the Rayleigh-Taylor instability (RTI) [12–14] is outstanding because it is easy to understand, not too difficult to rationalize, and also important in many technological and physical situations. The dispersion relation for regular gravity waves on a deep ocean reads $\omega = \sqrt{gk}$, where g is the downward gravity acceleration, $\omega/(2\pi)$ is the wave frequency, and k its horizontal wave number. As often noticed, if one turns the gravity upward, that is if one changes the sign of g, ω becomes purely imaginary $\pm i\sqrt{-gk}$, showing the existence of fluctuations growing exponentially with time. These fluctuations do not saturate and yield ultimately fingers of liquids in free fall. If one considers, as we do below, a soft solid in air with its surface turned downward, there are *a priori* good reasons to believe that some sort of RTI will set in. To figure it, consider a horizontal elastic slab of thickness h subjected to the gravity of Earth g, the upper surface being fixed to a rigid body, the lower one being free (Fig. 1). A sinusoidal perturbation $\zeta = \varepsilon \sin(kx)$ of the surface height (with x an in-plane coordinate) causes a reduction in the gravitational energy per unit area equal to $\frac{1}{2\lambda}\int_0^\lambda \rho g \zeta^2 dx = \frac{1}{4}\rho g \varepsilon^2$, where ρ is the mass density of the elastic medium and $\lambda = 2\pi/k$ is the wavelength. The corresponding elastic energy cost per unit volume scales as the shear modulus μ times the mean squared strain. In the long wave limit ($kh \ll 1$) the strain scales as ϵ/h: the sample is vertically squeezed from length h to $h - \varepsilon$ above a trough of the wave [region (a) of Fig. 1], it is vertically stretched above a peak from h to $h + \varepsilon$ [region (b)], and the deformation varies progressively in between [region (c)]. Finally, the mean elastic energy per unit volume scales as $h\mu(\varepsilon/h)^2$. Comparing the two contributions of the total energy, it appears that the Rayleigh-Taylor buoyancy

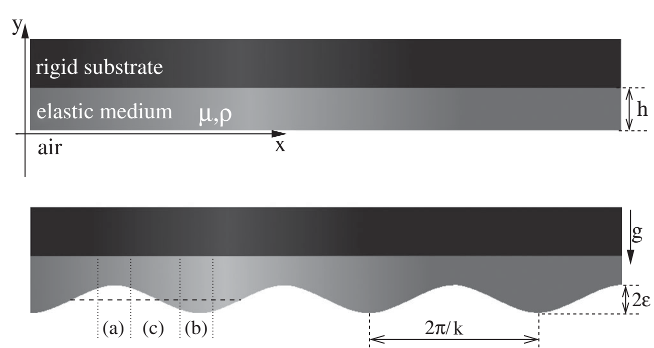

FIG. 1. Scheme of a sinusoidal disturbance of a downward facing and initially flat surface of a heavy elastic slab. The other surface is fixed on the rigid substrate. The energy change due to this disturbance can be positive or negative depending on the value of the dimensionless ratio $\rho gh/\mu$ with ρ the mass density, g the (gravitational) acceleration, h the thickness, and μ the elastic modulus.

overcomes elasticity beyond an instability threshold $\rho gh/\mu = \alpha^*$, where α^*, the dimensionless proportionality constant for the elastic energy (with a factor of 4), is to be found (see Supplemental Material [15], part B for the complete calculation).

In the same situation a thin layer of liquid is always unstable, which is equivalent to set to zero the shear modulus in the previous estimate. Therefore, contrary to liquids, RTI in a solid has a well-defined threshold for layers of finite thickness. Beyond it, the deformation increases up to a finite value for which the elastic cost balances the buoyancy gain: a steady state of equilibrium is then reached.

Although RTI in solids is expected to play a role in many fields such as biology, geology [16,17], or astrophysics [18], both a direct observation and a clear characterization are missing. In [19,20] and [21], a flat metal plate whose thickness is initially periodically modulated with a low amplitude is accelerated by expanding detonation products. The growth of the initial perturbation is observed through the use of x-ray shadowgraphs. It was found to be governed by the yield strength of the elastoplastic material, the initial amplitude, and the plate thickness. More recently, yogurts with a sinusoidal perturbation at the surface were put in a mold and accelerated using a linear electric motor. The stability regions of this elastic-plastic material have been investigated in terms of acceleration, amplitude, and wavelength of the initial perturbation [22]. In both cases (flat metal plate and yogurt), the observations consist of evolving states which are clearly associated to plastic deformations of preexisting periodic ripples at the free surface. Schematically, when the acceleration exerts a strong enough stress on the ripples, the yield stress of the material is overcome at the ripples extremities, which begin to flow. In the experiments of [22], the case of an initially flat surface has been briefly investigated. The authors reported the existence of a nonstationary surface instability and related its nucleation to the elastic (reversible) deformations of the material. Their conclusion seems erroneous insofar as it is based on a comparison with a theoretical expression valid for samples whose height is much higher than the wavelength, which is not the case in their experiments. The results obtained in the present Letter demonstrate unambiguously that if the phenomenon observed by these authors were a consequence of RTI for an elastic solid, their observations would have been different. It is therefore likely that the observed phenomenon is a consequence of the plastic properties of the investigated material.

Following the pioneering analytic work of Drucker [23], RTI in *plastic* solids has been modeled in the visco-elasto-plastic approximation in order to simulate the growth in amplitude of initial sinusoidal perturbations [24–26]. RTI for purely elastic plates with an initially flat surface has been analytically studied by Plohr and Sharp [27], whose results were generalized a few years after [28,29]. They predict for each value of the acceleration the existence of a critical perturbation wavelength beyond which the flat surface is unstable. As a consequence, an elastic plate is always unstable, provided its dimensions are large enough compared to the unstable wavelengths. This is in contrast with the instability studied in this Letter. On the other hand, Bakhrakh and Kovalev [30] have analytically studied the case of an accelerated elastic half space and found that it is unstable with respect to any perturbations with a wavelength larger than $4\pi\mu/(\rho g)$.

We report below the experimental observation of an instability occurring on the surface of a heavy ideal elastic solid pointing downwards. This instability occurs above a threshold and results in steady patterns. At threshold, elasticity exactly counterbalances buoyancy for an infinitesimal perturbation of the free surface. This phenomenon is closely related to Rayleigh waves [31] since the phase velocity of elastic surface waves decreases as the inward gravity increases. This provides a physical interpretation of the instability we have demonstrated, insofar as it occurs when the gravity is strong enough to make the phase velocity fully vanish. This viewpoint leads us straightforwardly to calculate the growth rate of the instability.

In our experiments, we use aqueous polyacrylamide gels consisting in a loose permanent polymer network immersed in water. The density of this incompressible elastic material is almost equal to that of water. It behaves as an elastic solid for strains up to several hundreds of percent (Supplemental Material [15], part A). The shear modulus can be tuned over a wide range by varying the concentrations in monomers and cross-linkers, or the temperature. In our experiments, it lies between 30 and 150 Pa. It is measured through indentation tests (Supplemental Material [15], part A).

The reagents generating the gel are dissolved in ultrapure water and poured into the brim in a cylindrical dish whose walls are covered with a thin layer of Velcro loops to prevent any further detachment. After the gel is made and its shear modulus measured, the dish is flipped upside down. Various methods have been tested: (i) reversal when the system is immersed in water (density close to that of the gel), the container is then gently removed out of the water keeping horizontal the free surface; (ii) reversal carried out in air but with a rigid plate keeping flat the surface during inversion. The plate is then gently removed; (iii) direct and fast flipping of the system in air without any special care. The three methods lead to identical results. The surface of the thinnest or the hardest samples remains perfectly flat [Fig. 2(a)]. In a narrow range of shear moduli and heights nonpropagating undulations grow spontaneously at the free surface of the gel and remain permanently [Figs. 2(b), 2(c), 2(d)]. For lower shear moduli or for greater thicknesses, several cuvettes appear next to each other at the surface, and remain permanently. For a constant thickness, their number (from one to seven in our experiments) and their

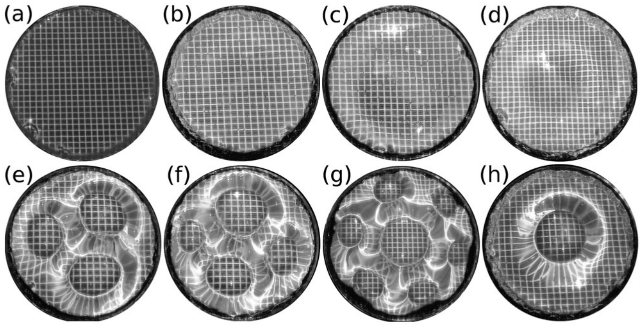

FIG. 2. Views of the downward facing free surface of gels with different shear moduli. (a) $\mu = 78\pm\ 0.5$ Pa, (b) 44 ± 0.5 Pa, (c) 43.3 ± 0.5 Pa, (d) 42.8 ± 0.5 Pa, (e) 41.0 ± 0.5 Pa, (f),(g), (h) 40.0 ± 0.5 Pa. The cylindrical dish is 18 cm diameter and 2.75 cm deep. (a)–(g) Steady patterns obtained just after reversal. (h) The sample temperature was 50° when reversed. The snapshot is taken after the sample has cooled to room temperature.

size depend on the shear modulus [Figs. 2(e), 2(f), 2(g)]. In any case, flipping again the container (so that the free surface is horizontal and upward) leads to the perfectly flat surface we started from. In addition, successive reversals lead to the same observations, except for a particular sample for which the number of cuvettes is either four, or seven [Figs. 2(f) and 2(g)]. We infer that the shear modulus of this sample corresponds to a threshold for the number of cuvettes so that the final configuration of the system is driven by uncontrolled external disturbances. This point is discussed at the end.

To obtain quantitative information about the surface deformation, a regular light grid is projected about the free surface [Fig. 3(a)]. The gel being transparent and the bottom of the container being white, the observed image of the grid results from one refraction followed by one reflection and another refraction. If the free surface is flat, this image corresponds to the grid without geometric distortion [Fig. 2(a)]. It is warped if the free surface is deformed, this distortion is bigger if the surface is more deformed [Fig. 2(b)—2(g)]. To measure the distortion, a rectangular lattice is fitted with the recorded images using the least squares method. The fitting parameters are a translation, the parameters and the orientation of the lattice, and a possible quadratic distortion taking into account the (small) radial decentering optical distortion [Fig. 3(b)]. Figure 3(c) shows this deviation plotted as a function of μ for samples having the same thickness $h = 2.75$ cm. Fitting functions $a + b(\mu - \mu^*)^c$ with these data gives $\mu^* = 44.6 \pm 1.8$ Pa, demonstrating the existence of an instability threshold at μ^* [Fig. 3(c)]. This threshold corresponds to a critical dimensionless acceleration $\alpha^* = (\rho g h/\mu^*) = 6.05 \pm 0.25$.

We expect that the onset of instability will show up when the frequency of a mode of propagation of elastic waves [31–33] at finite wavelength becomes zero. We consider an infinite layer of a heavy and incompressible elastic medium

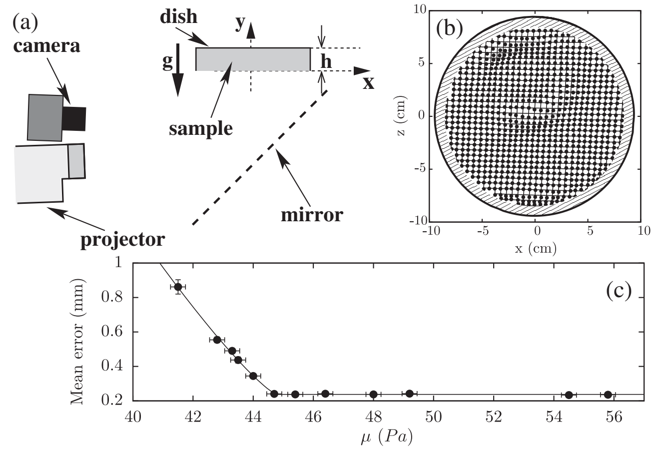

FIG. 3. Quantitative analysis of the surface distortion. (a) Experimental setup. The distance mirror-projector sample is 1.5 m while the dish diameter is 18 cm. (b) Full circles: intersections of the distorted lines of the grid observed on a sample ($\mu = 41.5 \pm 0.5$ Pa). Solid lines defined the grid that best fits the observed one. (c) Square root of the mean squared error with the grid that best fits the observed one as a function of μ with $h = 2.75$ cm (full circles). The solid line is the best fit with the power law $a + b(\mu^* - \mu)^c$. We find $\mu^* = 44.6 \pm 1.8$ Pa.

of thickness h with a free downward facing surface with air, the other surface being fixed on a rigid substrate. We also consider a plane wave propagating in the in-plane $\hat{x}$ direction (see Fig. 3) with the (small) displacement $\mathbf{u} = \mathbf{u}(y)e^{i\omega t - kx}$ (boldface being for vectors). Putting this displacement field in the equations of motion for an isotropic and incompressible heavy elastic medium [34,35] with the boundary conditions described just above, we obtain after linearization a condition for the dimensionless frequency $\tilde{\omega} = \omega h\sqrt{\mu/\rho}$ and the dimensionless wave number $\tilde{k} = kh$ (see Supplemental Material [15], part C):

$$\det\begin{pmatrix} 0 & 2\tilde{k}^2 & 0 & \tilde{s}^2 + \tilde{k}^2 \\ -\tilde{\omega}^2 + 2\tilde{k}^2 & -\alpha\tilde{k} & 2\tilde{k}\,\tilde{s} & -\alpha\tilde{k} \\ \tilde{k}\cosh\tilde{k} & -\tilde{k}\sinh\tilde{k} & \tilde{s}\cosh\tilde{s} & -\tilde{s}\sinh\tilde{s} \\ -\tilde{k}\sinh\tilde{k} & \tilde{k}\cosh\tilde{k} & -\tilde{k}\sinh\tilde{s} & \tilde{k}\cosh\tilde{s} \end{pmatrix} = 0, \tag{1}$$

for $\tilde{s}^2 = \tilde{k}^2 - \tilde{\omega}^2 > 0$. In Fig. 4, left, $\tilde{\omega}$ is plotted from Eq. (1) as a function of $\tilde{k}$ for various values of $\alpha = (\rho g\mu/h)$. The curves exhibit a local minimum for $\alpha > 4.5$, resulting in two possible wavelengths for one frequency. The frequency at the minimum becomes zero for $\alpha = \alpha^* = 6.223\cdots$: the propagation speed of the waves is then zero and a sinusoidal perturbation of the surface with the corresponding wave number is stationary. The surface is then linearly unstable. The theoretical value of α^* is in good agreement with experimental observations (Fig. 3). The finite size of our samples therefore has no

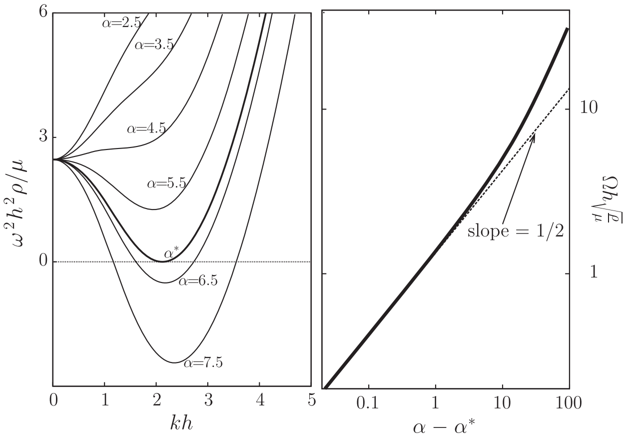

FIG. 4. Predictions for waves propagating at the surface of a heavy elastic material. Left: dimensionless frequency squared $\omega^2 h^2 \mu/\rho$ as a function of the dimensionless wave number kh for different values of α. For $\alpha < \alpha^*$, the flat surface is stable and ω is the Rayleigh frequency. For $\alpha > \alpha^*$ the flat surface is unstable and the growth rate of the most unstable mode is $\Omega = \sqrt{-\omega_{\min}^2}$, $\omega_{\min}$ being the minimum of ω. Right: Dimensionless growth rate of the mode k with the maximum growth rate obtained from Eq. (1) as a function of the gap with the instability threshold (solid line).

significant effect on the threshold value, nor the gel-air interfacial tension, which is consistent with the calculation of supplement-B in the Supplemental Material [15]. Furthermore $\tilde{k} = 2.12$ with $h = 2.75$ cm corresponds to 8 cm for the wavelength, consistent with snapshots (b) and (c) of Fig. 2. For $\alpha > \alpha^*$ we find $\omega^2 < 0$. Writing $\omega = i\Omega$, we obtain the growth rate Ω of the instability (Fig. 4, right). We find $\Omega \simeq \sqrt{(1.8\mu/\rho h^2)}\sqrt{\alpha - \alpha^*}$ for $\alpha \leq 1.3\alpha^*$, corresponding to a characteristic time $(1/\Omega)$ ranging from 0.2 [sample (b) of Fig. 2] to 0.1 s [sample (g)]. Unfortunately, such a characteristic time cannot be experimentally measured since it is shorter than the duration required to place the sample.

The preceding theoretical study applies for infinitesimally small strains, i.e., near the threshold. Well beyond it, the final patterns are obtained after a substantially longer duration [a few seconds for patterns of Figs. 2(e), 2(f), 2(g)]. A surprising and striking nonlinear feature of the instability is the difference in the observed patterns between snapshots 2(f),2(g), and 2(h) of Fig. 2, all the three corresponding to the same shear modulus with the same container size. The first two are directly obtained from a gel of 40 ± 0.5 Pa at room temperature. The third one is obtained after cooling sample of Figs. 2(f) and 2(g) upside down from 50 degrees down to room temperature. The shear modulus correspondingly decreases from 44 ± 0.5 Pa to 40 ± 0.5 Pa. The cooling takes place gradually from the boundaries towards the center of the sample, resulting in shear modulus gradients until thermal equilibrium is reached. The dramatic difference between the observed patterns highlights the existence of several equilibrium configurations. This must be related to a complicated energy landscape with several local minima far from the instability threshold, providing a particularly interesting challenge for non linear physics and morphogenesis. Somehow the notion of instability as introducing a kind of free choice in the evolution of a system shows up here. It implies that the ultimate state reached after such an instability depends not only on the growth of the unstable structure itself but also on uncontrollable or at least hard to control small effects, like various inhomogeneities in space and time. This is clearly evidenced in our experiment.

We have shown that RTI exists in real elastic solids and that it can be observed in everyday's gravity field in soft hydrogels. The instability threshold depends on the shear modulus, the thickness and the density of the sample. Our experimental set-up with soft elastic gels has enabled a quantitative comparison with a linear theory. This has allowed us to identify the basic ingredients of this instability and the way it appears. Measuring the dispersion relation of surface waves can be a mean to detect the proximity of the threshold, and therefore to predict an impending change.

These results open the way for further fundamental studies, for instance concerning the dynamic formation and the large-scale organization of the patterns, which are both of great importance for non linear physics and morphogenesis. RTI in solids should also be found in more complex situations, such as biology, geology and industrial processing, with visco-plastic, visco-elastic or non-isotropic materials. Moreover, the instability is expected to occur in more extreme conditions (high accelerations, strong and non-uniform gravitational fields) where the direct observation is hardly possible. We believe that our work lays foundation to address such more complex cases.

The authors are indebted to E. Bouchaud and M. Destrade for interesting discussions. This work has been supported by the French National Research Agency (ANR) under Contract No. ANR-2010-BLAN-0402-1 (F2F).

*smora@univ-montp2.fr

[1] K. Shull, C. Flanigan, and A. Crosby, Appl. Phys. Lett. **84**, 3057 (2000).

[2] M. Adda-Bedia and L. Mahadevan, Proc. R. Soc. A **462**, 3233 (2006).

[3] S. Mora, T. Phou, J. M. Fromental, L. M. Pismen, and Y. Pomeau, Phys. Rev. Lett. **105**, 214301 (2010).

[4] S. Mora, M. Abkarian, H. Tabuteau, and Y. Pomeau, Soft Matter **7**, 10612 (2011).

[5] J. Dervaux and M. B. Amar, Annu. Rev. Condens. Matter Phys. **3**, 311 (2012).

[6] R. Style, C. Hyland, R. Boltyanskiy, J. Wettlaufer, and E. Dufresne, Nat. Commun. **4**, 2728 (2013).

[7] B. Saintyves, O. Dauchot, and E. Bouchaud, Phys. Rev. Lett. **111**, 047801 (2013).
[8] J. Biggins, B. Saintyves, Z. Wei, E. Bouchaud, and L. Mahadevan, Proc. Natl. Acad. Sci. U.S.A. **110**, 12545 (2013).
[9] T. Tallinen, J. S. Biggins, and L. Mahadevan, Phys. Rev. Lett. **110**, 024302 (2013).
[10] S. Mora, C. Maurini, T. Phou, J. M. Fromental, B. Audoly, and Y. Pomeau, Phys. Rev. Lett. **111**, 114301 (2013).
[11] R. W. Style, R. Boltyanskiy, Y. Che, J. S. Wettlaufer, L. A. Wilen, and E. R. Dufresne, Phys. Rev. Lett. **110**, 066103 (2013).
[12] Lord Rayleigh, Proc. London Math. Soc. **s1-14**, 170 (1882).
[13] G. I. Taylor, Proc. R. Soc. A **201**, 192 (1950).
[14] D. H. Sharp, Physica (Amsterdam) **12D**, 3 (1984).
[15] See Supplemental Material at http://link.aps.org/supplemental/10.1103/PhysRevLett.113.178301 for mechanical properties of the elastic materials and theoretical analysis.
[16] G. A. Houseman and P. Molnar, Geophys. J. Int. **128**, 125 (1997).
[17] E. B. Burov and P. Molnar, Earth Planet. Sci. Lett. **275**, 370 (2008).
[18] O. Blaes, R. Blandford, P. Madau, and S. Koonon, Astrophys. J. **363**, 612 (1990).
[19] J. F. Barnes, P. J. Blewett, R. G. McQueen, K. A. Meyer, and D. Venable, J. Appl. Phys. **45**, 727 (1974).
[20] J. F. Barnes, D. H. Janney, R. K. London, K. A. Meyer, and D. H. Sharp, J. Appl. Phys. **51**, 4678 (1980).
[21] A. I. Lebedev, P. N. Nizovtsev, V. A. Raevskii, and V. P. Solovev, Dokl. Akad. Nauk SSSR **349**, 332 (1996).
[22] G. Dimonte, R. Gore, and M. Schneider, Phys. Rev. Lett. **80**, 1212 (1998).
[23] D. C. Drucker, Ingenieur-Archiv **49**, 361 (1980).
[24] J. W. Miles, Defense Technical Center, p. 7335 (1960).
[25] J. W. Swegle and A. C. Robinson, J. Appl. Phys. **66**, 2838 (1989).
[26] A. I. Abakumov, A. I. Lebedev, I. A. Nizovtseva, P. N. Nizovtsev, and V. A. Rayevsky, VANT. Ser. Teor. i Prikl. Fizika **3**, 14 (1990).
[27] B. J. Plohr and D. H. Sharp, Z. Angew. Math. Phys. **49**, 786 (1998).
[28] G. Terrones, Phys. Rev. E **71**, 036306 (2005).
[29] A. R. Piriz, J. J. Lopez Cela, and N. A. Tahir, Phys. Rev. E **80**, 046305 (2009).
[30] C. Bakhrakh and N. Kovalev, *The 5th All-Union Conference on Numerical Methods of Solving Problems in the Theory of Elasticity and Plasticity, Novosibirsk, 1978* (Nauka Publishing House, Moscow, 1978), p. 15.
[31] L. J. Rayleigh, Proc. London Math. Soc. **s1–17**, 4 (1885).
[32] B. A. Bromwich, Proc. London Math. Soc. **30**, 98 (1899).
[33] F. Gilbert, Bull. Seismol. Soc. Am. **57**, 783 (1967).
[34] *Theory of Elasticity*, edited by L. D. Landau and E. M. Lifshitz (Pergamon Press, Oxford, 1981).
[35] M. Kuipers and A. A. F. van de Ven, Acta Mech. **81**, 181 (1990).